Open Journal of Fluid Dynamics, 2025, 15(4), 222-235
https://www.scirp.org/journal/ojfd
ISSN Online: 2165-3860
ISSN Print: 2165-3852

Numerical Solutions of 2-D Laminar Free Convection in an Isoceles Triangular Cavity Filled with a Darcy-Brinkman Porous Medium: Effect of Heat Source Size

Giovani Elie Baptista Malomar, Omar Ngor Thiam, Cheikh Mbow

Department of Physics, Faculty of Science and Technology, University Cheikh Anta Diop, Dakar, Senegal
Email: giovanielie.malomar@ucad.edu.sn, omarngor.thiam@ucad.edu.sn, mbowy@yahoo.com

How to cite this paper: Malomar, G.E.B., Thiam, O.N. and Mbow, C. (2025) Numerical Solutions of 2-D Laminar Free Convection in an Isoceles Triangular Cavity Filled with a Darcy-Brinkman Porous Medium: Effect of Heat Source Size. *Open Journal of Fluid Dynamics*, **15**, 222-235.
https://doi.org/10.4236/ojfd.2025.154013

Received: August 30, 2025
Accepted: December 13, 2025
Published: December 16, 2025

Abstract

In this work, a numerical study of free convection in an isoceles porous triangular cavity with a partially heated horizontal base and cooled upper walls is analysed. The uniform heat source is located centrally at the base wall. Darcy-Brinkman model is used; it is also assumed that the fluid used is incompressible and obeys the Boussinesq approximation. The non-dimensionless governing equations, stream function-vorticity, momentum and energy are discretized by finite difference method and solved using the successive over-relaxation (SOR) method. Streamline and isotherm patterns were presented at different lengths of heater ($0.25 \le \epsilon \le 1$), Darcy number ($10^{-4} \le Da \le 10^{-2}$), Prandtl number ($0.7 \le Pr \le 7$) and for different Rayleigh number ($10^3 \le Ra \le 10^6$). On the basis of the results, it is observed that the presence of a localized heat source may slightly accelerate the flow, but does not change the fundamental mode of convection. Beyond the critical value of Rayleigh number, the average Nusselt number characterizing overall heat transfer increases rapidly with decreasing source size.

Keywords

Free Convection, Partially Heating, Porous Media, Numerical Study

1. Introduction

The natural convection in confined porous media saturated by fluid is fundamental in the fields of engineering and physics. This interest arises from the importance of this heat transfer mode in various engineering fields such as storage of the thermal energy, solar energy collectors, thermal design for the buildings, cooling of electronic components (Alves and al. [1]; Kuznetsov and al. [2]; Sheremet and al. [3]), the underground spread of pollutants (Bagchi and al. [4]). The literature on the convective flow in porous media is abundant. An excellent review of most of these studies is in the books (Nield and al. [5]; Pop and al. [6]; Vafai [7]; Ingham and al. [8]) that give a complete overview of the current state of research in this area.

In many studies, rectangular enclosures have been chosen for the study of natural convection in both fluid and porous media. In addition to rectangular cavities, triangular cavities are of paramount importance in many applications, particularly in the building industry. Triangular cavities filled with air have been studied to simulate thermo-convective transfers in buildings [9]-[14]. However, the number of studies on triangular cavities filled with a porous medium is limited and generally focuses on right-angled triangular cavities [15]-[18], with Darcy's model often being used. These studies have highlighted the impact of the cavity's aspect ratio and Rayleigh number. In our work, we examine natural convection in isosceles triangular cavities. A few studies have been conducted in such a configuration [19]-[22].

Basak *et al.* [19] used finite element analysis to study the effects of uniform and non-uniform heating of the base wall on natural convection flows in isosceles triangular enclosures filled with porous media. The detailed analysis was performed in two cases based on different thermal boundary conditions: 1) two inclined walls are maintained at a constant cold temperature while the bottom wall is uniformly heated; 2) two inclined walls are maintained at a constant cold temperature while the bottom wall is heated non-uniformly. The numerical results are presented in terms of current functions, temperature profiles, and Nusselt numbers. It is observed that for small Darcy numbers, heat transfer is mainly due to conduction regardless of Pr. As the Darcy number increases, there is a shift from the dominant conduction regime to the dominant convection regime. Non-uniform heating of the lower wall produces a higher heat transfer rate at the center of the lower wall than uniform heating, but the average Nusselt number indicates a lower overall heat transfer rate for non-uniform heating.

In [20], Basak *et al.* investigate numerically the phenomena of natural convection in an isosceles triangular enclosure filled with a porous matrix. A penalty finite element analysis with bi-quadratic elements is used for solving the Navier-Stokes and energy balance equations. The detailed study is carried out in two cases depending on various thermal boundary conditions; Case I: two inclined walls are uniformly heated while the bottom wall is isothermally cooled and Case II: two inclined walls are non-uniformly heated while the bottom wall is isothermally cooled. It has been found that at low Darcy numbers, the heat transfer is primarily due to conduction irrespective of the Ra and Pr. As Rayleigh number increases, there is a change from conduction conduction-dominant region to convection dominant region for ($Da = 10^{-3}$), and the critical Rayleigh number corresponding to on-set of convection is obtained. Some interesting features of stream function and isotherm contours are discussed especially for low and high Prandtl number limits.

Varol *et al.* [21] examined heat transfer by natural convection in triangular enclosures filled with porous media and subjected to different boundary conditions. Six different cases were tested based on all possible boundary conditions for temperature on the vertical, bottom, and inclined walls of the enclosure. Based on the results, they observed that when the heating device was located on the bottom wall, multiple vortices formed, and the highest heat transfer was achieved compared to the other cases.

In [22], Varol *et al.* investigated numerical analysis of the entropy production has been performed due to natural convection heat transfer and fluid flow in isosceles triangular enclosures with partially heated from below and symmetrically cooled from sloping walls. It is observed that entropy production number increases but Bejan number decreases with increasing of Rayleigh number. However, both entropy production due to heat transfer and fluid friction irreversibility are affected by higher inclination angle of triangle and length of heater.

The main objective of this study is to numerically examine the effects of natural convection within a porous isocele triangular cavity subjected to localized heat sources. The Darcy-Brinkman model in the Boussinesq approximation is used to model the flow within the porous medium. The influences of the heat source size and Rayleigh number were studied.

2. Materials and Methods

2.1. Basic Equations

A schematic geometry of the problem is shown in **Figure 1**, where x' and y' are the cartesian coordinates, H' is the height of the cavity, L' the length of the base of the cavity and ϵ' the length of heater isothermal source. This is a triangular porous cavity two-dimensional and the rest of the non heated portions of the base wall are assumed to be thermally adiabatic. All walls of the cavity are assumed to be impermeable. At the same, bottom wall is partially or completely heated with a centrally located isothermal heat source T'_h and inclined walls are isothermally cooled at a constant temperature T'_c. The Boussinesq approximation is employed. Isotropy, homogeneity and local thermal equilibrium in the porous medium are assumed.

Under these assumptions, the dimensionless forms of governing equations for steady free convection flow in porous medium are (see Nield and Bejan [5]):

$$\frac{\partial^2\psi}{\partial x^2}+\frac{\partial^2\psi}{\partial y^2}=-\omega \tag{1}$$

$$\frac{\partial\psi}{\partial y}\frac{\partial\omega}{\partial x}-\frac{\partial\psi}{\partial x}\frac{\partial\omega}{\partial y}=\phi Pr\left(\frac{\partial^2\omega}{\partial x^2}+\frac{\partial^2\omega}{\partial y^2}\right)-\frac{\phi^2 Pr}{Da}\,\omega+Ra\phi^2 Pr\frac{\partial T}{\partial x} \tag{2}$$

$$\frac{\partial\psi}{\partial y}\frac{\partial T}{\partial x}-\frac{\partial\psi}{\partial x}\frac{\partial T}{\partial y}=\frac{\partial^2 T}{\partial x^2}+\frac{\partial^2 T}{\partial y^2} \tag{3}$$

where the Rayleigh, Darcy and Prandtl numbers are,

$$Ra=\frac{g\beta L'^3\left(T'_h-T'_c\right)}{\nu\alpha} \tag{4}$$

$$Da = \frac{K}{L'^2} \tag{5}$$

$$Pr = \frac{\nu}{\alpha} \tag{6}$$

The relationships between the dimensionless variables of equations (Equations (1)-(3)) and their dimensional counterparts are:

$$(x, y) = \left(\frac{x'}{L'}, \frac{y'}{L'}\right);\ (u, v) = \left(\frac{u'L'}{\alpha}, \frac{v'L'}{\alpha}\right);\ T = \frac{T' - T'_c}{T'_h - T'_c} \tag{7}$$

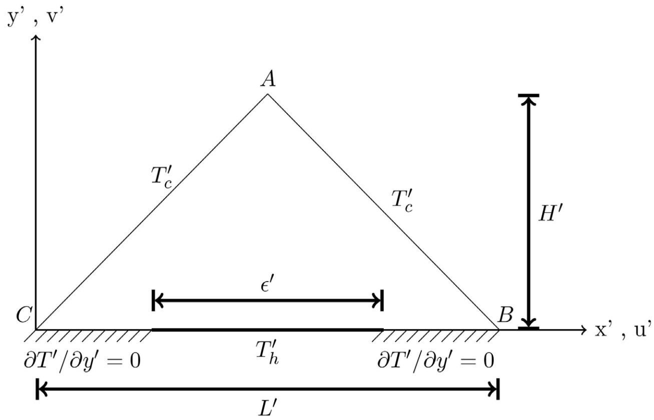

Figure 1. Schematic diagram of the physical model and coordinate system.

The relationships between dimensionless stream function, ψ, vorticity, ω and velocity components u and v are,

$$\omega = \frac{\partial v}{\partial x} - \frac{\partial u}{\partial y} \tag{8}$$

$$u = \frac{\partial \psi}{\partial y} \text{ and } v = -\frac{\partial \psi}{\partial x} \tag{9}$$

Equations (1)-(3) are associated with the following dimensionless boundary conditions

$$\begin{cases} \psi = 0;\ \omega = 0;\ T = 0 \text{ initial conditions} \\ \psi = 0 \text{ on three side} \\ T = T_c = 0 \text{ on side AB and AC} \\ T = T_h = 1 \text{ for } \dfrac{1-\epsilon}{2} \le x \le \dfrac{1+\epsilon}{2} \text{ on BC} \\ \dfrac{\partial T}{\partial y} = 0 \text{ for } 0 \le x \le \dfrac{1-\epsilon}{2} \text{ and } \dfrac{1+\epsilon}{2} \le x \le 1 \text{ on BC} \end{cases} \tag{10}$$

where ϵ is the dimensionless heat source length, defined by $\epsilon = \frac{\epsilon'}{L'}$.

For calculating the vorticity values at the boundary points, we use Thom's formula [23].

Heat Transfer

Once as the temperature field is known, we may define the heat transfer coefficient in terms of local Nusselt number, Nu from the heated portion of the base wall by

$$Nu = -\left(\frac{\partial T}{\partial y}\right)_{y=0} \tag{11}$$

However, this local Nu is unbounded at the corners of triangular cavity where the hot base meets the cold side walls when the bottom wall is completely heated. Therefore, determination of an average Nu characterizing the heat transfer would be unbounded at the tip region. So, to get an idea of the evolution of the average Nusselt number when the base is fully heated, we determined it when the base is almost fully heated ($\epsilon = 0.95$), and Figure 8 confirms that our approach is acceptable.

On the hot wall, the average Nusselt number is determined by:

$$\overline{Num} = -\int_{\frac{1-\epsilon}{2}}^{\frac{1+\epsilon}{2}} \left(\frac{\partial T}{\partial y}\right)_{y=0} \mathrm{d}x \tag{12}$$

2.2. Numerical Method

The governing equations (Equations (1)-(3)) associated with the boundary conditions (Equation (10)) are discretized by a finite difference scheme, centred and forward accurate to the second order and first order, respectively. The three equations in stream function-vorticity and temperature formulation are then solved using successive over-relaxation (SOR) method. We note that we have used the same relaxation parameter when we update the stream function, vorticity and temperature values. Uniform grids have been selected in both the x and y direction. We have developed a numerical code with Fortran 95.

During iterations, the calculation stops when between two iterations, the following conditions are satisfied by the stream function, vorticity and temperature,

$$\max\left(\left|R_\psi\right|\right) \le 10^{-8} \text{ and } \max\left(\left|R_\omega\right|\right) \le 10^{-5} \text{ and } \max\left(\left|R_T\right|\right) \le 10^{-8} \tag{13}$$

Here, R_ψ, R_ω and R_T are the residual of the steady state stream function, vorticity and temperature equations (Equations (1)-(3)). We define this residual as the following,

$$R_\psi = \frac{\psi_{i+1,j} - 2\psi_{i,j} + \psi_{i-1,j}}{\Delta x^2} + \frac{\psi_{i,j+1} - 2\psi_{i,j} + \psi_{i,j-1}}{\Delta y^2} + \omega_{i,j} \tag{14}$$

$$\begin{aligned} R_\omega = {} & \phi Pr\left(\frac{\omega_{i+1,j} - 2\omega_{i,j} + \omega_{i-1,j}}{\Delta x^2} + \frac{\omega_{i,j+1} - 2\omega_{i,j} + \omega_{i,j-1}}{\Delta y^2}\right) \\ & - \frac{\phi^2 Pr}{Da}\omega_{i,j} + Ra\phi^2 Pr\left(\frac{T_{i+1,j} - T_{i-1,j}}{2\Delta x}\right) \\ & + \frac{\left(\psi_{i+1,j} - \psi_{i-1,j}\right)\left(\omega_{i,j+1} - \omega_{i,j-1}\right)}{4\Delta x\Delta y} \\ & + \frac{\left(\psi_{i,j-1} - \psi_{i,j+1}\right)\left(\omega_{i+1,j} - \omega_{i-1,j}\right)}{4\Delta x\Delta y} \end{aligned} \tag{15}$$

$$
\begin{aligned}
R_T = & \frac{T_{i+1,j} - 2T_{i,j} + T_{i-1,j}}{\Delta x^2} + \frac{T_{i,j+1} - 2T_{i,j} + T_{i,j-1}}{\Delta y^2} \\
& + \frac{\left(\psi_{i+1,j} - \psi_{i-1,j}\right)\left(T_{i,j+1} - T_{i,j-1}\right)}{4\Delta x \Delta y} \\
& + \frac{\left(\psi_{i,j-1} - \psi_{i,j+1}\right)\left(T_{i+1,j} - T_{i-1,j}\right)}{4\Delta x \Delta y}
\end{aligned}
\tag{16}
$$

Preliminary tests on the influence of the mesh have allowed us to retain a uniform mesh size of 120*60 for all simulation. The present numerical code has been validated against the works of Basak and al. [19].

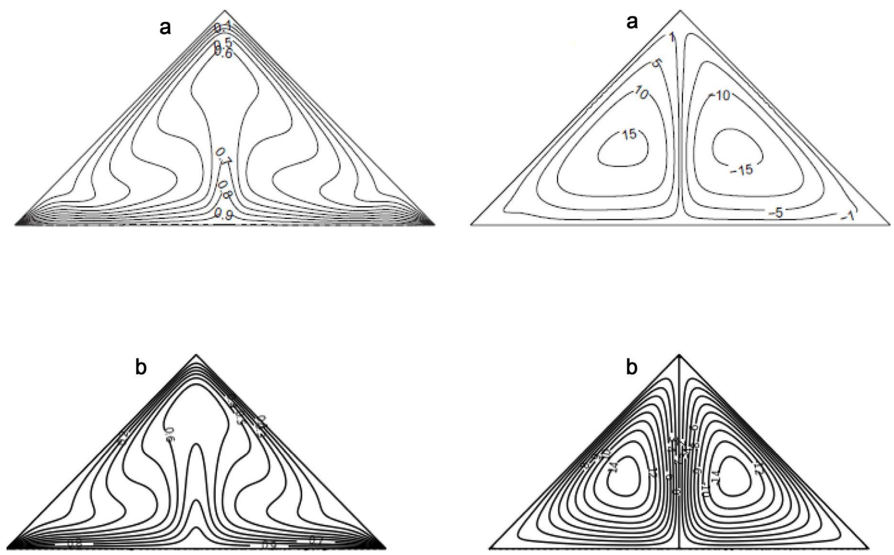

Figure 2. Streamline and isotherm for $\epsilon = 1$, $Ra = 10^6$, $Da = 10^{-3}$, $Pr = 0.7$. (a) Basak; (b) Our work.

3. Results and Discussion

3.1. Symmetric Flow and Temperature Field

In the field of control parameters of the problem cited above, we have noticed that the computed flow and temperature field remain symmetric with respect to the geometric midplane (see **Figures 2-6**). The flow rises in the center of the cavity and falls along each cold inclined side creating mirror image structures that rotate clockwise in the right half and counterclockwise in the left half. It is noted that the horizontal component of velocity is zero everywhere along the vertical centerline of the cavity.

3.2. Effect of Heat Source Size

In order to clearly understand the effects of having a localized heat source at the bottom wall and the effects of the Rayleigh number, we represented in **Figures 3-6** streamline and isotherms patterns for $\epsilon = 1, 0.95, 0.5$ and 0.25, $Da = 10^{-3}$, $Pr = 7$ respectively at different Rayleigh numbers ($Ra = 10^3$ - 10^6).

For $\epsilon = 1$, when the bottom wall is uniformly heated, there is no convective motion at $Ra = 10^3$ and the system is in the conduction mode. It is observed that the gradient of the stream function is extremely low. Structure of isotherms confirms that heat transfer is primarily due to conduction. When Ra increases to 10^5 convective motion begins, streamline patterns show that the gradient of the stream function is small but not negligible, which indicates that a circulatory fluid motion with low velocity exists. However, there is competition between the conductive and convective modes at this Rayleigh number, and this fluid movement does not significantly improve the overall rate of heat rate, as shown in **Figure 7**. The structure of the isotherms shows a slight rise of a thermal plume. When Ra increases to 2.5×10^5, convective motion dominate as illustrate by the gradient of the stream function who is relatively high. The corresponding isotherms show a rising thermal plume. With further increase in Ra to 10^6 the convective motion becomes intense and the isotherm patterns show a narrow thermal plume rising along the centerline of the cavity.

When the size of the heating source covers only half the base, *i.e.* $\epsilon = 0.5$, **Figure 5** shows that the stream functions are similar to those in case those of the $\epsilon = 1$ case, except at $Ra = 10^3$ and $Ra = 10^5$, where the maximum values of the stream function are higher. This phenomenon can be explained by the fact that at the ends of the heating source, there is a horizontal thermal gradient which accelerates fluid circulation. This phenomenon has also been observed in the convection

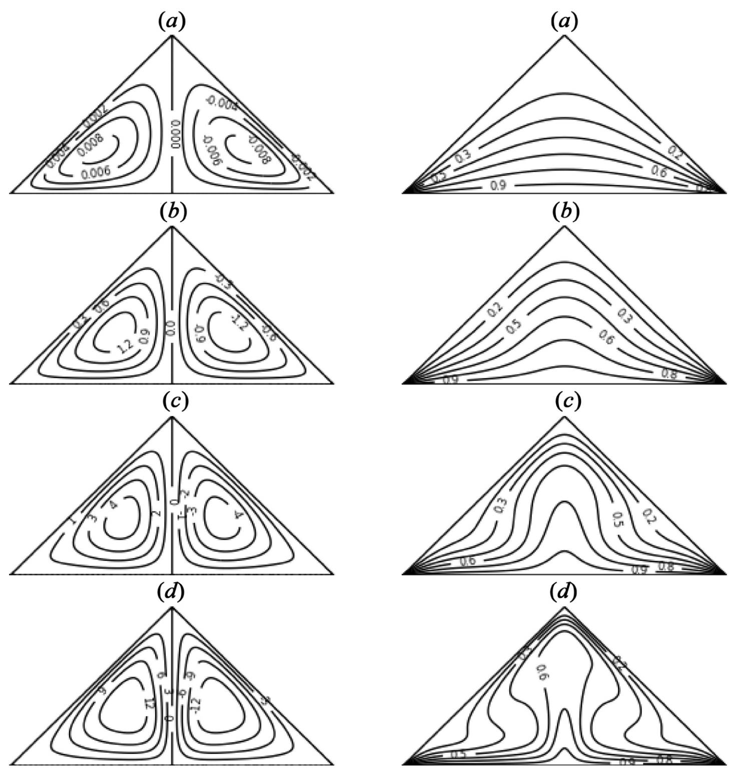

Figure 3. Streamline and isotherm for $\epsilon = 1$, $Da = 10^{-3}$, $Pr = 7$. (a) $Ra = 10^3$, (b) $Ra = 10^5$, (c) $Ra = 2.5 \times 10^5$, (d) $Ra = 10^6$.

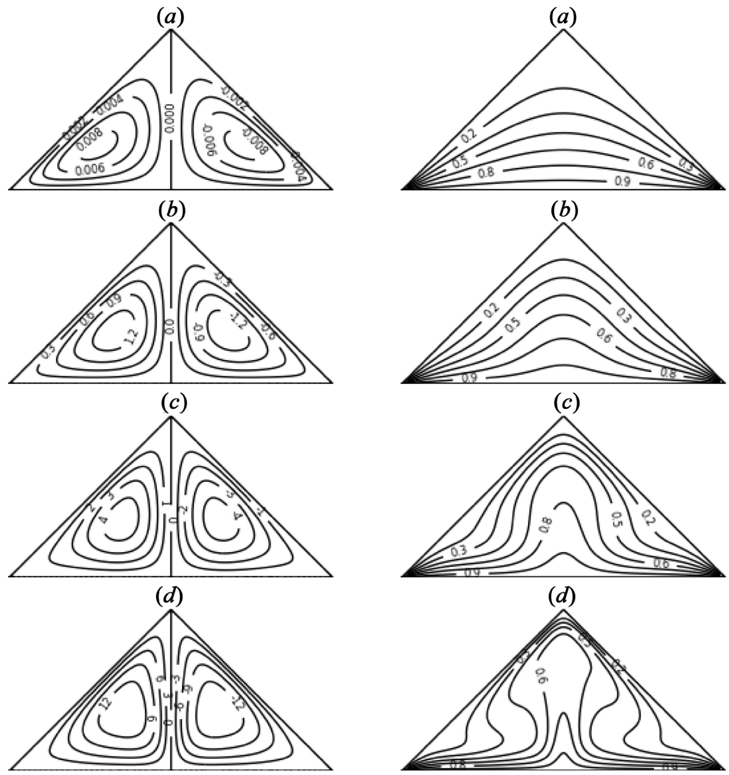

Figure 4. Streamline and isotherm for $\epsilon = 0.95$, $Da = 10^{-3}$, $Pr = 7$. (a) $Ra = 10^3$, (b) $Ra = 10^5$, (c) $Ra = 2.5 \times 10^5$, (d) $Ra = 10^6$.

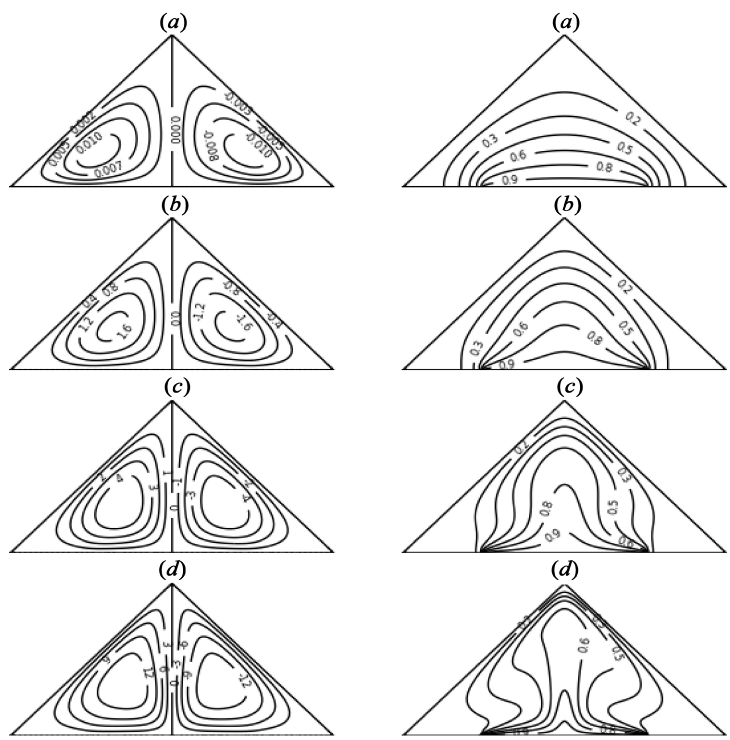

Figure 5. Streamline and isotherm for $\epsilon = 0.5$, $Da = 10^{-3}$, $Pr = 7$, (a) $Ra = 10^3$, (b) $Ra = 10^5$, (c) $Ra = 2.5 \times 10^5$, (d) $Ra = 10^6$.

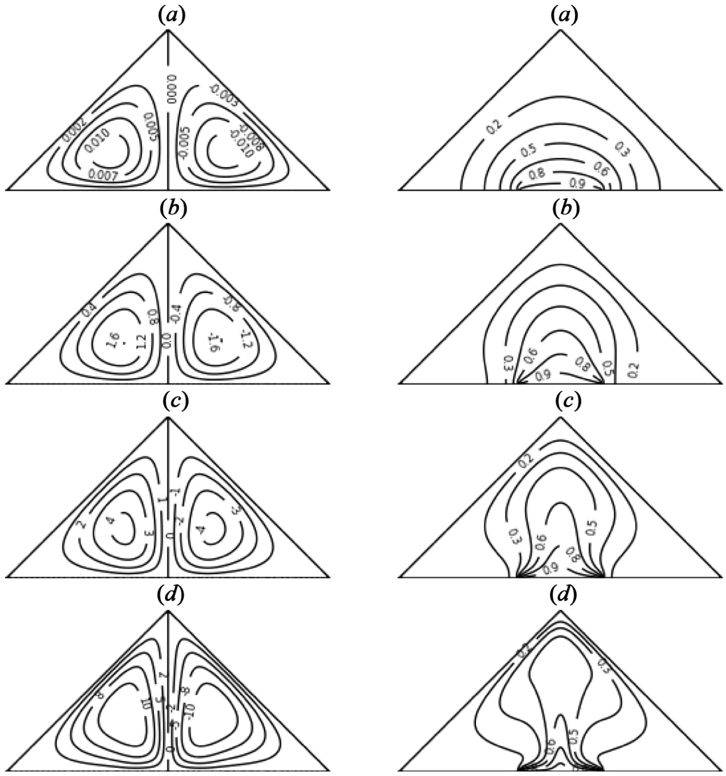

Figure 6. Streamline and isotherm for $\epsilon = 0.25$, $Da = 10^{-3}$, $Pr = 7$, (a) $Ra = 10^3$, (b) $Ra = 10^5$, (c) $Ra = 2.5 \times 10^5$, (d) $Ra = 10^6$.

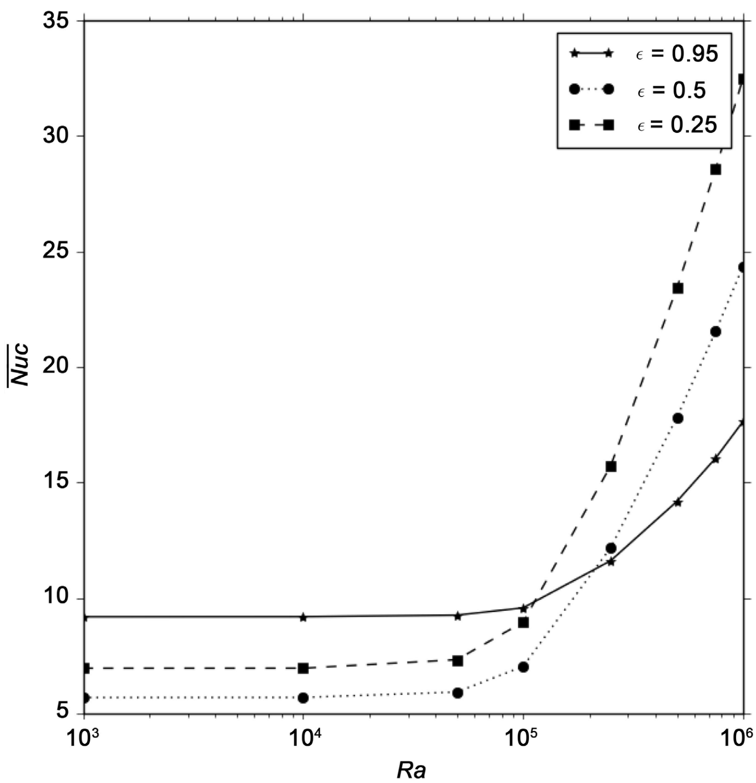

Figure 7. Evolution of $\overline{Nuc}$ as a function of Ra for different ϵ.

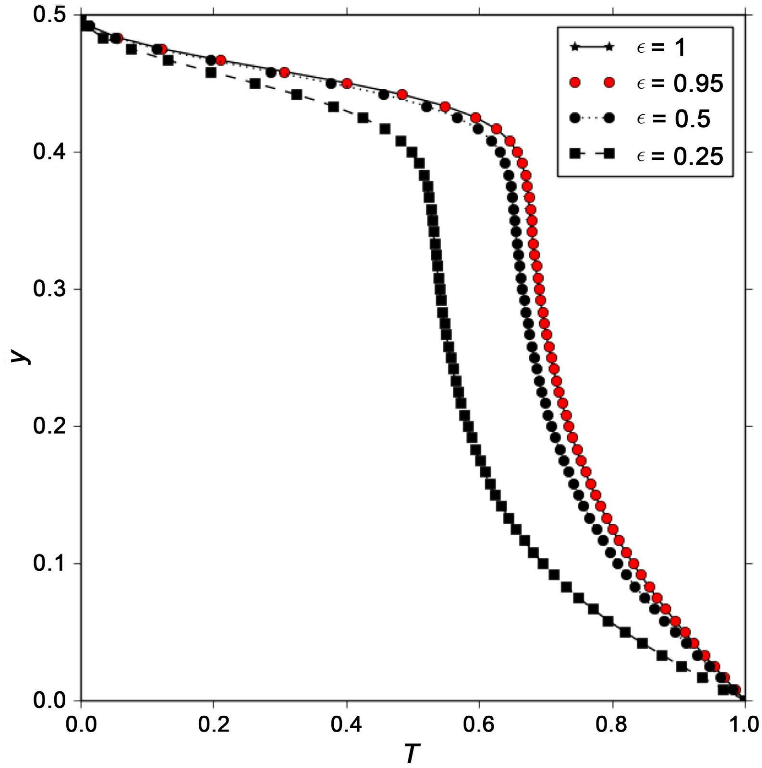

Figure 8. Temperature profile along the vertical axis of cavity symmetry for different ϵ, $Ra = 10^6$, $Da = 10^{-3}$, $Pr = 7$.

in porous layers with localized heat sources, [24]. We also noticed that with the increase in Ra, the thermal plume rising above the heat source becomes narrow, as in the case of $\epsilon = 1$ case.

A further decrease in the size of the heat source to $\epsilon = 0.25$ shows largely similar characteristics to those described above, *i.e.* for $\epsilon = 0.5$. As Ra increases, the isotherm profile shows a rising thermal plume and quantitatively similar streamlines to those for $\epsilon = 0.5$. We have noted that, for high values of Ra, whatever the streamlines remain quantitatively similar, which shows that the flows are not affected by the size of the heating source at high Rayleigh numbers. In view of the results, we can say that the presence of the localized heat source may slightly accelerate the flow but does not change the fundamental mode of convection. The effect of the localized heat source on overall heat transfer is illustrated in **Figure 7**. When the base is almost completely heated, the critical Rayleigh number for the onset of convection is approximately of $Ra_c \simeq 7.10^4$. Below this critical value of Rayleigh number, heat transfer is by conduction. We also note that below this value, the value of Nusselt number remains almost constant. However, when the heat source is localized, at low Ra numbers, the Nusselt numbers obtained remain close to those obtained when the base is almost uniformly heated. At $Ra = 10^3$, the presence of the discrete heat source initiates a circulatory movement of the fluid due to the existence of a horizontal thermal gradient at the ends of the source.

However, this circulatory movement remains weak, resulting in a domination of the conductive mode, as illustrated by the structure of the isotherms, **Figure 5** and **Figure 6**. **Figure 7** also shows that even for discrete heat sources, the Nusselt number remains approximately constant until the critical point is reached. At $Ra = 10^3$, regardless of ϵ heat transfer takes place by conduction. Beyond the critical point Ra_c, we note an interesting aspect, average Nusselt number on the hot end increases rapidly with decreasing heat source size. This can be explained by the fact that in the case of a discrete heat source, the major part of the heating zone is included in the central region, through which the heat is discharged, and consequently almost all of the heat input is removed by convection.

With a further reduction of ϵ, almost all the energy supplied is dissipated by convective flow. As a result, with a further decrease in the size of the source, the energy input at the base is transferred upwards by convection. We can therefore deduce that a localized heat source is more efficient at channeling energy input to the heat source via the thermal plume, leading to higher average Nusselt numbers for shorter heating lengths beyond the critical point.

Finally, to conclude on the effects of a localized heat source, the temperature profiles along the vertical axis of symmetry of the cavity are shown at $Ra = 10^6$, $Da = 10^{-3}$, $Pr = 7$ and for different ϵ as shown in **Figure 8**. It can be seen that as the size of the heating source decreases, the temperature profiles along the axis of symmetry of the thermal plume change significantly from $\epsilon = 0.5$ to $\epsilon = 0.25$. We note that for a given *y*, the temperature decreases as the size of the heat source decreases and this is true for temperatures throughout the cavity. These results can be understood by analyzing the structure of the isotherms. As the size of the heat source decreases, a large part of the temperature drop along the plume occurs very close to the heating source, while in the rest of the plume, the temperature changes progressively. This is due to the fact that decreasing size of the heat source, the plume takes up more and more of the heat which is supplied to the system.

4. Conclusions

This study investigated the numerical analysis of natural laminar convection within a porous isocele triangular cavity subjected to localized heat sources. The Darcy-Brinkman model in the Boussinesq approximation was used to model the flow within the porous medium. The influences of the size of the heat source and the Rayleigh number were studied. The main conclusions are as follows:

- It is observed that the presence of a localized heat source can slightly accelerate the flow but does not change the fundamental mode of convection.
- Beyond the critical point, the average Nusselt number which characterizes the overall heat transfer, increases rapidly as the size of the source decreases.
- A localized heat source is more effective at channeling energy to the heat source via the upward thermal plume, leading to higher average Nusselt numbers for shorter heating lengths beyond the critical point.

Acknowledgements

We thank the editor and the reviewers for their comments.

Conflicts of Interest

The authors declare no conflicts of interest regarding the publication of this paper.

References

[1] Alves, T.A. and Altemani, C.A.C. (2012) An Invariant Descriptor for Heaters Temperature Prediction in Conjugate Cooling. *International Journal of Thermal Sciences*, **58**, 92-101. https://doi.org/10.1016/j.ijthermalsci.2012.03.007

[2] Kuznetsov, G.V. and Sheremet, M.A. (2008) New Approach to the Mathematical Modeling of Thermal Regimes for Electronic Equipment. *Russian Microelectronics*, **37**, 131-138. https://doi.org/10.1134/s1063739708020078

[3] Sheremet, M.A. and Pop, I. (2014) Natural Convection in a Square Porous Cavity with Sinusoidal Temperature Distributions on Both Side Walls Filled with a Nanofluid: Buongiorno's Mathematical Model. *Transport in Porous Media*, **105**, 411-429. https://doi.org/10.1007/s11242-014-0375-7

[4] Bagchi, A. and Kulacki, F.A. (2013) Natural Convection in Superposed Fluid-Porous Layers, Springer Briefs in Applied Sciences and Technology. Springer.

[5] Nield, D.A. and Bejan, A. (2017) Convection in Porous Media, Volume 3. Springer.

[6] Pop, I. and Ingham, D.B. (2001) Convective Heat Transfer: Mathematical and Computational Modelling of Viscous Fluids and Porous Media. Pergamon.

[7] Kambiz, V. (2015) Handbook of Porous Media. CRC Press.

[8] Ingham, D.B. and Pop, I. (2005) Transport Phenomena in Porous Media III. Elsevier Science.

[9] Asan, H. and Namli, L. (2000) Laminar Natural Convection in a Pitched Roof of Triangular Cross-Section: Summer Day Boundary Conditions. *Energy and Buildings*, **33**, 69-73. https://doi.org/10.1016/s0378-7788(00)00066-9

[10] Holtzman, G.A., Hill, R.W. and Ball, K.S. (2000) Laminar Natural Convection in Isosceles Triangular Enclosures Heated from Below and Symmetrically Cooled from Above. *Journal of Heat Transfer*, **122**, 485-491. https://doi.org/10.1115/1.1288707

[11] Asan, H. and Namli, L. (2001) Numerical Simulation of Buoyant Flow in a Roof of Triangular Cross-Section under Winter Day Boundary Conditions. *Energy and Buildings*, **33**, 753-757. https://doi.org/10.1016/s0378-7788(01)00063-9

[12] Akinsete, V.A. and Coleman, T.A. (1982) Heat Transfer by Steady Laminar Free Convection in Triangular Enclosures. *International Journal of Heat and Mass Transfer*, **25**, 991-998. https://doi.org/10.1016/0017-9310(82)90074-6

[13] Ridouane, E.H., Campo, A. and Hasnaoui, M. (2006) Benefits Derivable from Connecting the Bottom and Top Walls of Attic Enclosures with Insulated Vertical Side Walls. *Numerical Heat Transfer*, *Part A*: *Applications*, **49**, 175-193. https://doi.org/10.1080/10407780500302257

[14] Kpode, K., Sow, M.L. and Mbow, C. (2016) Unsteady Natural Convection with Summer Boundary Conditions in a Habitat at High Rayleigh Number and at High Time. *Energy and Buildings*, **121**, 72-77. https://doi.org/10.1016/j.enbuild.2016.03.068

[15] Poulikakos, D. and Bejan, A. (1983) Numerical Study of Transient High Rayleigh Number Convection in an Attic-Shaped Porous Layer. *Journal of Heat Transfer*, **105**,

476-484. https://doi.org/10.1115/1.3245610

[16] Varol, Y., Oztop, H.F. and Varol, A. (2007) Natural Convection in Porous Triangular Enclosures with a Solid Adiabatic Fin Attached to the Horizontal Wall. *International Communications in Heat and Mass Transfer*, **34**, 19-27. https://doi.org/10.1016/j.icheatmasstransfer.2006.09.004

[17] Varol, Y., Oztop, H.F. and Varol, A. (2007) Free Convection in a Triangular Porous Media Filled Enclosure Heated or Cooled Horizontal and Vertical Walls. *The* 3*rd International Energy*, *Exergy and Environment Symposium*, Évora, 1-5 July 2007.

[18] Varol, Y., Oztop, H.F. and Varol, A. (2006) Free Convection in Porous Media Filled Right-Angle Triangular Enclosures. *International Communications in Heat and Mass Transfer*, **33**, 1190-1197. https://doi.org/10.1016/j.icheatmasstransfer.2006.08.008

[19] Basak, T., Roy, S. and Krishna Babu, S. (2008) Natural Convection and Flow Simulation in Differentially Heated Isosceles Triangular Enclosures Filled with Porous Medium. *Chemical Engineering Science*, **63**, 3328-3340. https://doi.org/10.1016/j.ces.2008.03.038

[20] Basak, T., Roy, S., Babu, S.K. and Pop, I. (2008) Finite Element Simulations of Natural Convection Flow in an Isosceles Triangular Enclosure Filled with a Porous Medium: Effects of Various Thermal Boundary Conditions. *International Journal of Heat and Mass Transfer*, **51**, 2733-2741. https://doi.org/10.1016/j.ijheatmasstransfer.2007.10.009

[21] Varol, Y., Oztop, H.F. and Varol, A. (2008) Free Convection Heat Transfer and Flow Field in Triangular Enclosures Filled with Porous Media. *Journal of Porous Media*, **11**, 103-115. https://doi.org/10.1615/jpormedia.v11.i1.70

[22] Varol, Y., Oztop, H.F. and Koca, A. (2008) Entropy Production Due to Free Convection in Partially Heated Isosceles Triangular Enclosures. *Applied Thermal Engineering*, **28**, 1502-1513. https://doi.org/10.1016/j.applthermaleng.2007.08.013

[23] Weinan, E. and Liu, J.G. (1996) Vorticity Boundary Condition and Related Issues for Finite Difference Schemes. *Journal of Computational Physics*, **124**, 368-382.

[24] Poulikakos, D., Bejan, A., Selimos, B. and Blake, K.R. (1986) High Rayleigh Number Convection in a Fluid Overlaying a Porous Bed. *International Journal of Heat and Fluid Flow*, **7**, 109-116. https://doi.org/10.1016/0142-727x(86)90056-1

Nomenclature

g	Gravity intensity, m·s^{-2}
K	Permeability of the porous medium, m^2
T	Dimensionless temperature
(x, y)	Dimensionless coordinates
(u, v)	Dimensionless velocitu components along x and y axes
Ra	Rayleigh number for porous medium
Da	Darcy number
Pr	Prandtl number
Nu	local Nusselt number, at the heated base wall
$\overline{Nuc}$	Average Nusselt number, at the heated base wall

Greek Symbols

α	Effective thermal diffusivity, m^2·s^{-1}
β	Coefficient of thermal expansion, K^{-1}
ν	kinematic viscosity, kg·m^{-1}·s^{-1}
ϕ	Porosity of porous media
ϵ	dimensionless heat source length ω Vorticity
ψ	Dimensionless stream function
ρ_0	Reference density of fluid, kg·m^{-3}

Superscript

(‘)	Dimensional variables
(-)	Average values

Subscript

c	Cold
h	Hot